Supplementary Material – Strain Localisation

S1 Strain Localisation – Ductile Fracture

Zr-alloys and austenitic Ni-alloys and stainless steels are used in reactor cores because of their high strength and toughness. They retain sufficient toughness for operability after irradiation in power reactors to high doses. Unlike ferritic and ferritic-martensitic steels that are easily embrittled by irradiation at very low doses compared with Zr alloys and austenitic alloys [1], Figure S1.

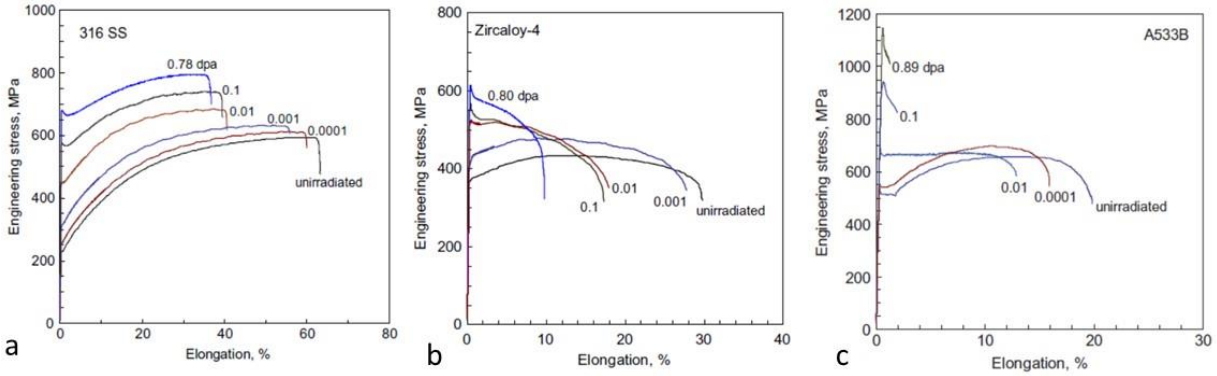

Figure S1. Effect of irradiation on the stress-strain behavior for: (a) 316 stainless steel; (b) Zircaloy-4; and (c) A533B pressure vessel steel. Irradiation was in the Hydraulic Tube Facility of the High Flux Isotope Reactor at 65 °C – 100 °C to the doses indicated for each plot. Reprinted/adapted with permission from [1], 2006, Elsevier.

Ferritic steels may retain sufficient toughness for operation at high temperatures, but they also exhibit a ductile-to-brittle transition at low temperatures, unlike Zr alloys and austenitic alloys, Figure S2 [2]. Ferritic steels are used for pressure vessels and for pressurized piping because of their high yield strengths but they are not used within the core region because of embrittlement at low neutron fluences. If the operating temperature is high as it is for fast reactors, and will be for Gen IV reactors, then ferritic alloys may be used with less concern except if there is an expectation that the components must still function (not fracture) if the temperature is reduced.

Austenitic alloys are used in the cores of fast reactors (for the internals and as fuel cladding) because they retain toughness after irradiation and the absorption of thermal neutrons does not limit operability. Light water reactors can tolerate some austenitic usage in the core because they operate with some enrichment of U^{235} in the fuel (3% – 5%), but the fuel cladding is made from Zr-alloys to maintain a sufficiently high thermal neutron flux near the fuel.

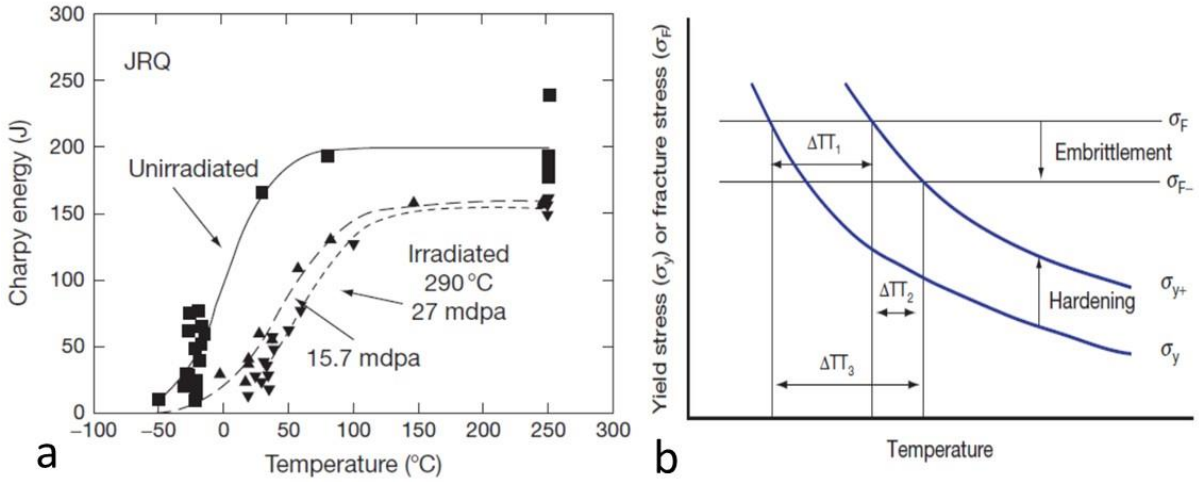

Figure S2: (a) Effect of irradiation on the Charpy-V upper shelf energy of the JRQ material (A508 cl.3 forging) irradiated in a materials test reactor to doses of 15.7 and 27 mdpa (1 mdpa = 0.001 dpa); (b) Shift in DBTT due to irradiation of a typical RPV steel. In (b) the effect of irradiation is to increase the yield stress, σ_y, and decrease the fracture stress, σ_F. The total temperature shift in fracture strength is caused by both hardening (ΔTT_1) and other factors such as element segregation (ΔTT_2). The combined effect is a larger shift to higher temperatures (ΔTT_3). Reprinted/adapted with permission from [2], 2012, Elsevier.

Nuclear reactors that operate using natural uranium (about 0.7% U^{235}) as fuel can only do so by maintaining a high thermal neutron flux, which makes up for the lower concentration of fissionable material. This high thermal neutron flux is maintained by using heavy water or graphite as the moderator. For the CANDU reactor, which operates using natural uranium, heavy water is also used for the coolant and most of the internals are constructed using Zr-alloys. The containment vessel is made from 304 stainless steel. Neutron absorbing elements such as Ni-alloys are restricted to small, specialized components such as springs and flux detectors, Figure S3 [3]. Thus, although the fast neutron flux is greatly diminished at the edge of the reactor core, the thermal neutron flux is still high (note neutron spectra also shown in Figure S3 (a)). A CANDU 6 reactor contains 380 fuel channels. A single fuel channel consists of a 6m long Zr-2.5Nb pressure tube that has an internal diameter of about 104 mm and a wall thickness of about 4.2 mm. It is attached to a 403 ferritic/martensitic steel end-fitting that is out of the core (Fgure S3(b)). The end-fitting is not fixed but moves on bearings that accommodate the dimensional changes that occur from pressure and temperature changes during start-up and shut-down of the reactor. More importantly the bearings allow for fuel channel expansion over the life of the reactor caused by irradiation creep, which is anisotropic. The fuel channel has a closed-end and thus if the pressure tubes had an isotropic creep response there would be no elongation. Because thermal creep is more-or-less isotropic [4], it is only because creep occurring during irradiation is anisotropic that the bearings need sufficient travel to allow for irradiation creep.

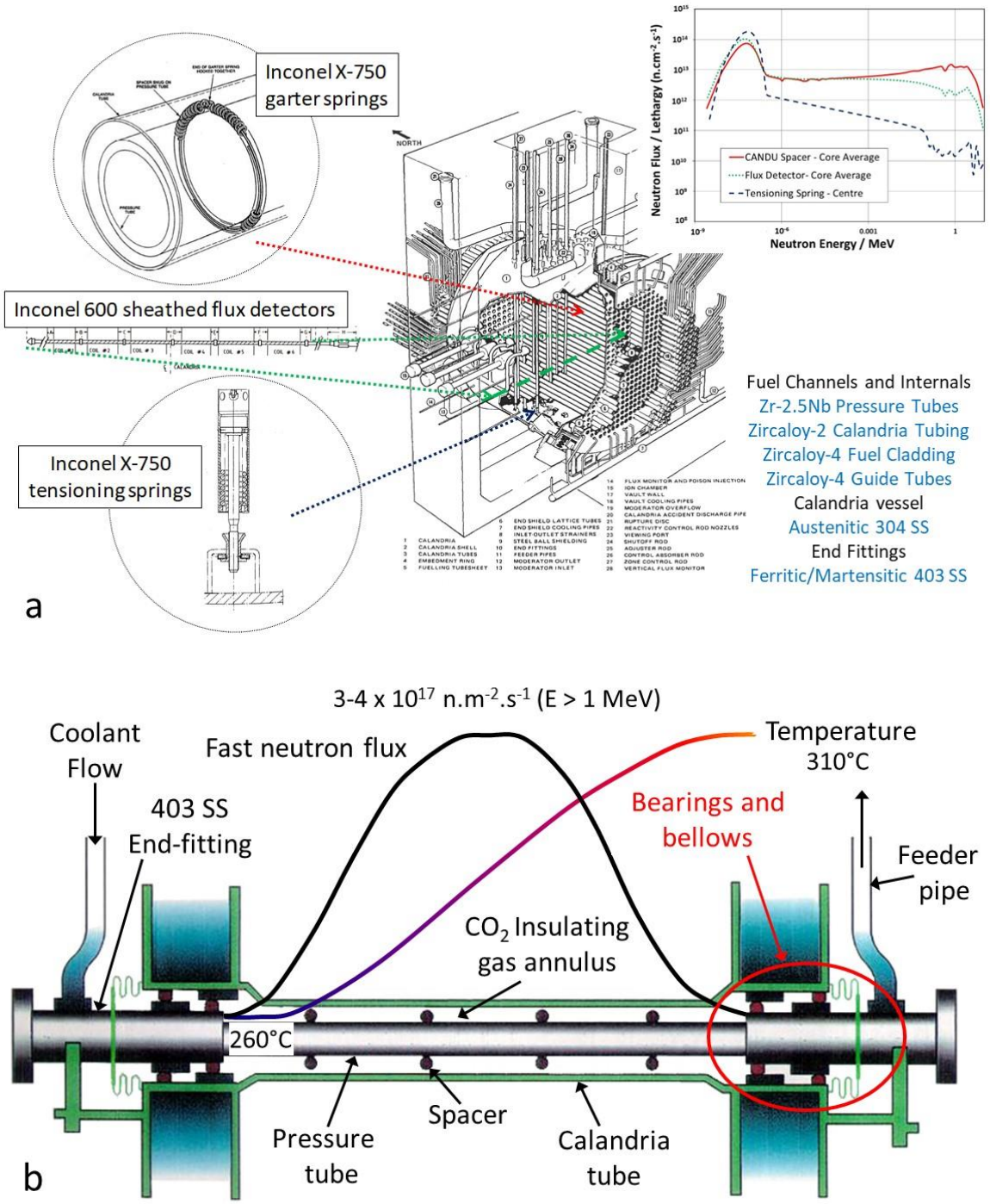

Figure S3. (a) schematic showing materials in a CANDU reactor.; (b) schematic showing a single fuel channel illustrating how the calandria tube is fixed to the reactor vessel (304 SS) and the pressure tube is in a closed-end configuration. Reprinted/adapted with permission from [3], 2022, Elsevier.

Based on in-reactor creep tests using creep capsules at a temperature of about 280 °C for stresses between 100 MPa and 150 MPa (applicable to reactor operation), the in-reactor transverse strain

rate in the hoop direction is approximately double that in the axial direction [5]. The hypothetical anisotropy factors chosen to match the relative strain rates are (F=0.7, G=0.15, H=0.15). Note that this is for creep during irradiation and is a different anisotropy to that expected for yielding of pressure tubing in a closed end burst test and has a different scaling factor (k) that determines the magnitude of the tensor representation quadric (see main text). In that case the hypothetical anisotropy factors for plastic deformation were derived to be consistent with a measured yield stress ratio of about 1.4 [6] are (F=0.45, G=0.05, H=0.5), with k varied to match experimental measurements in the longitudinal and transverse directions. The hypothetical plane stress tensor quadrics for plastic and irradiation creep deformation are illustrated in Figure S4. Note that, for the case where the compliance tensor representation quadric is applied to yielding of an isotropic material, then F=G=H=0.5 if k is chosen to be the yield stress, i.e. the Von Mises condition. Also shown is the case for isotropic material for comparison. For a pressure tube during irradiation in a closed-end configuration the relative creep rates are given by the normal to the surface at the intersection with the biaxial stress locus. The same radius normal intercept for the isotropic material as shown in Figure S4 indicates that the axial deformation is zero.

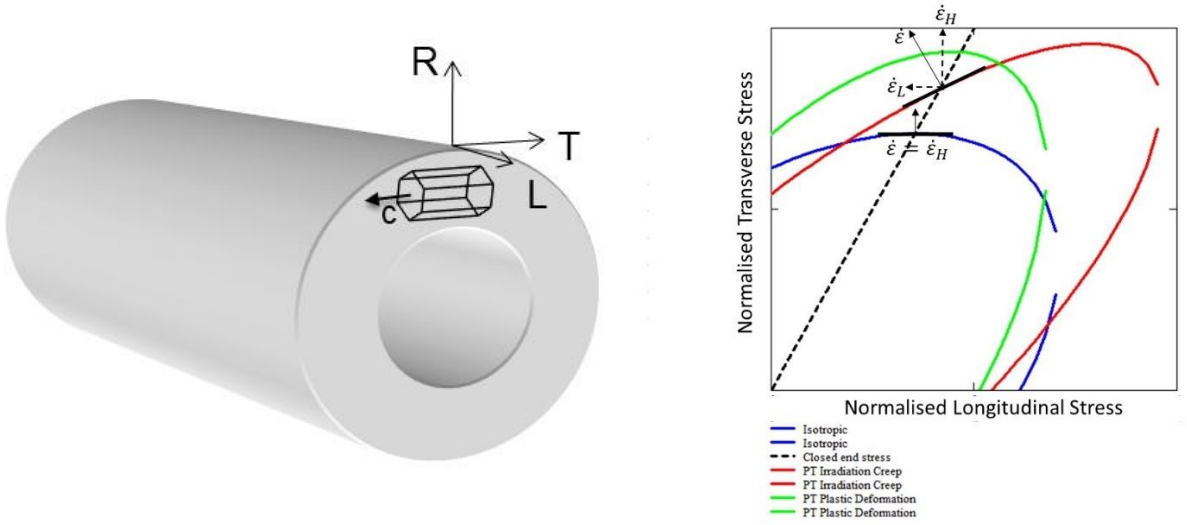

Figure S4. Composite showing preferred orientation for a pressure tube and the corresponding creep compliance tensor quadric for planar stress in the longitudinal (L) and transverse (T) plane that is perpendicular to the radial (R) direction. Different stress loci intersect the surfaces defined by the tensor for the plane stress condition ($\sigma_R \cong 0$) as shown. With increasing pressure in a closed-end tube the stress locus is shown by the black dotted line. The radial-normal vector at the intersection with the surface for an isotropic material (blue curve) shows that there is no axial strain. The radial-normal vector at the intersection with the surface representing irradiation creep (red curve) shows that the axial strain rate is about half of the transverse (hoop) strain rate. The green plot shows the surface for plastic deformation of an unirradiated pressure tube.

S2 Strain localisation in IASCC

Strain localisation by channeling is often cited as being correlated with irradiation assisted SCC (IASCC) by linking the initiation stress and density of channels with observations of SCC. For 4-point bends tests on solution-annealed 304 SS irradiated with neutrons in the BOR-60 reactor at 320 °C, the stress level has been expressed as a fraction of the irradiated yield stress for room temperature tests by Gussev et al. [7] (Figures S5) and for boiling water reactor (BWR) normal water chemistry (NWC) conditions at 288 °C by Stephenson and Was [8] (Figures S6). Gussev states that yield stresses are 0.2% values [7] and presumably the same applies to the data of Stephenson et al. [8]. The yield stress values used by Gussev et al. were derived from spherical indentation tests [7] and presumably the same method applied to the results of Stephenson et al. [8]. For the data of Gussev et al. [7], the stress values where channels were first observed (see figure S5) closely coincide with the true yield stress range for 316L SS (571 MPa – 674 MPa) measured by Byun et al. [9]. Note that Byun et al. also stated that twinning in their irradiated material was initiated at a stress of 600 MPa, i.e. 40 MPa lower than the stress measured for the onset of channeling (640 MPa).

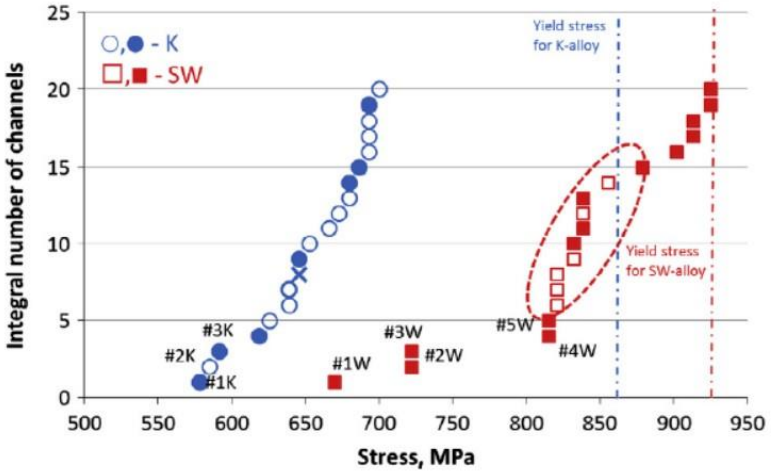

Figure S5. Integral number of observed channels in a given area for the investigated alloys as a function of stress. Filled symbols indicate cases where the channel origin points were located at the middle of the grain boundary and as a rule close to stiff grain (>210 MPa); open symbols indicate channels that started at triple junction points. Reprinted/adapted with permission from [7], 2015, Elsevier.

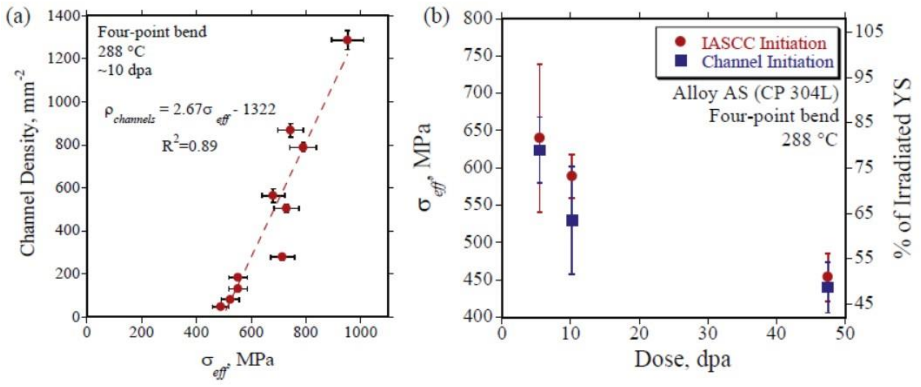

Figure S6. (a) Stress dependence of channel density for ~10 dpa irradiated conditions during elastic deformation, and (b) average stress (and approximate % of the irradiated yield stress on the right vertical axis) to initiate DCs and initiate IASCC in neutron irradiated solution-annealed 304 SS a function of irradiation dose. Reprinted/adapted with permission from [8], 2016, Elsevier.

The mechanism by which channels promote SCC in irradiated materials was described by Stephenson and Was [8] and illustrated in Figure S7 for the case of SCC initiating at a manganese sulphide inclusion.

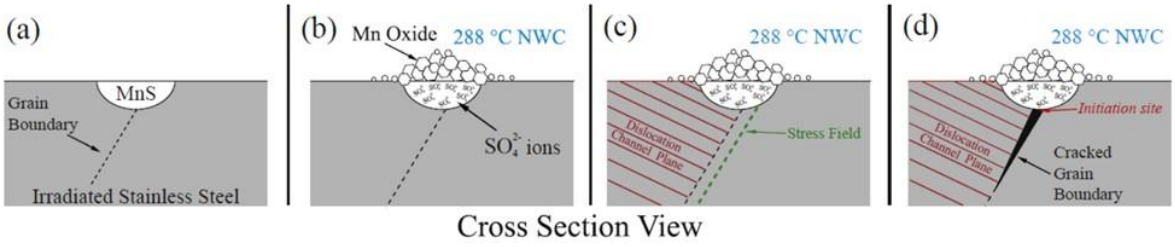

Figure S7. IASCC initiation caused by a dissolving MnS inclusion and a stress field formed by a discontinuous DC intersecting the incident GB. a) A MnS inclusion at a grain boundary prior to exposure, b) after exposure to NWC, the MnS oxide dissolves to form an oxide cap which occludes the inclusion site and attracts SO4 2, c) a discontinuous dislocation channel intersects the grain boundary at the inclusion site, creating a field of high stress, and d) IASCC initiates at this site. Reprinted/adapted with permission from [8], 2016, Elsevier.

In their model Stephenson and Was [8] associate stresses created by the impingement of dislocation channels on grain boundaries with crack initiation. In their case the cracking mechanism is somewhat ambiguous. It is not clear whether the stress field where shear bands run into a boundary is deemed sufficient to initiate a crack, which is highly unlikely (see main text), or whether the existence of a dislocation channel at a grain boundary allows for some additional mechanism to create a crack. The ambiguity whether the channels are, in fact twins, is an additional cause for confusion. Whereas one would anticipate that stress inhomogeneities will coincide with material inhomogeneities when a material is plastically deformed, the need to invoke channeling is not immediately clear. Stress inhomogeneities are an inevitable outcome of plastic deformation. Dislocation channeling, like twinning, is a bulk shear and therefore the

conditions to get the type of stress amplification at the head of a slip band (a planar shear) needed to create a Stroh-type crack [10] do not apply. It could be argued that channeling first creates a region that is free of dislocations within which planar slip could be activated as noted by Gussev et al. [7], but that only increases the complexity and adds to the convoluted nature and ambiguity of the cracking mechanism.

Different authors have invoked the observations of small misorientations in the vicinity of features deemed to be channels (either at the edge of the features or where they intersect a boundary) as a means of promoting the notion that high stresses exist in these volumes. Dislocation pile up at an interface that is in the form of a polygonised wall (sub-grain boundary), rather than at the head of a planar slip band (see Figures 10 and 11 in the main text), would also result in a local misorientation observed in diffraction mode and cannot be ruled out in these cases [11, 12] given the lack of detailed microstructure analyses.

Channeling is a mechanism that accounts for lower ductility and a load drop (coincident with localised softening) of irradiated material that fails in a ductile manner. There is no obvious reason why channeling by itself is necessary to initiate cracking at a grain boundary, especially as there are many examples of channeling in irradiated materials where impingement at grain boundaries does not create a crack (see main text). Therefore, the need for an initiation site from localised oxidation is paramount. When cracks advance in metals, they do so by emitting dislocations (unless it is a cleavage crack). Emission of dislocations will also blunt the crack and promote deformation perpendicular to, rather than parallel to, the crack plane. If the emission of dislocations is restricted to the crack tip that would help initiate and maintain a sharp crack. It is conceivable that the presence of softer dislocation free channels could restrict dislocation emission from an incipient or corrosion-induced crack to narrow bands within which the critical resolved shear stress (CRSS) is lower than the surrounding material and that could be a mechanism for promoting crack advance, especially if the stress concentration from the crack itself promoted additional shear in softer channels ahead of the crack. In that case it would not be the stress caused by channel impingement at the boundary that is important, rather the creation of softer zones that promote the initiation and allow for crack advance.

S4 Strain Localisation – Inter-granular and Trans-granular Fracture

Although ductile failure is the most common failure mode for engineering alloys even after irradiation (Figure S1), the increase in strength and reduction in ductility generally saturates at a low dose (<1 dpa for Zr-1lloys and < 5 dpa for austenitic alloys) corresponding with the saturation in the dislocation loop density [4, 5]. When helium is being generated, however, mechanical properties such as ultimate tensile strength and ductility are reduced and inter-granular failure is observed primarily because of the segregation of He-stabilised bubbles on grain boundaries. This feature of He embrittlement is best demonstrated by the extreme example provided by Braski [13], see supplementary material in [14]. The difference between He-embrittlement and the embrittlement caused by hardening of the matrix (resulting in flow localization in narrow channels) is that the latter process involves an increase in the yield and ultimate tensile strength of the material (Figure S1). It is the reduced volume of material that is deforming in a softened channel that results in eventual failure at lower bulk engineering strains,

but high local strains in the channels. He-embrittlement, however, reduces the strength of the material by weakening grain boundaries so that failure is easier, and cracks therefore propagate, along the boundaries, Figures S9. The crack propagation probably involves dislocation slip rather than decohesion because the grain boundary is complex and decohesion has little meaning compared with a process such as cleavage, which does involve decohesion at a sharp crack. A hypothetical slip-based fracture mode is shown in Figure S9.

Although it is difficult to retroactively track the fracture path to particular features in the microstructure after bulk testing, micro-tensile tests afford better control and one can more easily link certain features to fracture paths. Focussed ion beam milling is another advance in materials testing and characterisation that provides a means of easily associating crack localization with particular features in the microstructure. Micro-tensile and mini-tensile tests of neutron or ion irradiated materials containing high densities of He-stabilised bubbles have shown that trans-granular fracture progesses primarily along the interface with large twin/martensite platelets [15]. It has been observed that He bubbles also segregate at these interfaces, see main text and supplementary material in [14], and therefore it is possible that He-bubble segregation at trans-granular platelets is an additional factor determining trans-granular failure.

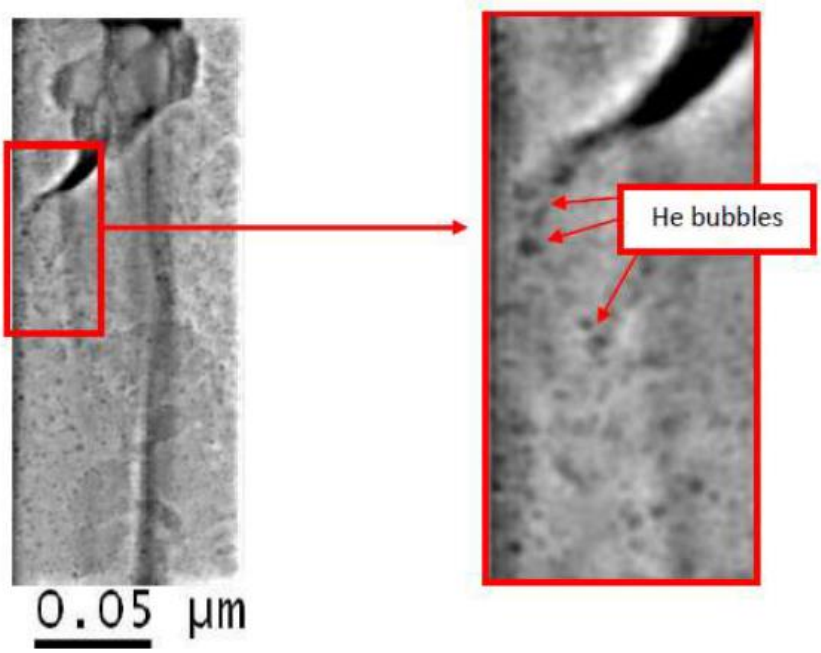

Figure S8. A TEM micrograph of irradiated Inconel X-750 spacer material showing a crack along a grain boundary. Reprinted/adapted with permission from [3], 2022, Elsevier.

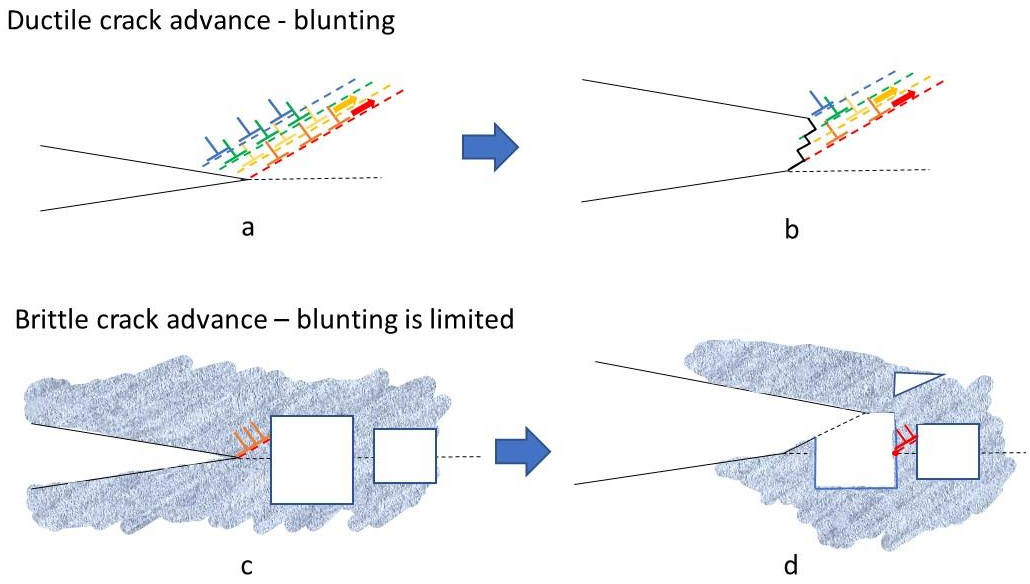

Figure S9. Schematic diagram showing how cavities restrict the volume for dislocation translation thus limiting the absorbed energy for crack advance (lowering fracture toughness). The stress at the hinge points (red dots) will be dependent on the area of the ligament up to the nearest free surface (cavity): (a) crack on a boundary/interface subject to a crack-opening load (F); (b) crack blunting and energy absorption due to dislocation emission; (c) restricted dislocation emission (lower energy absorption for crack advance) and lower applied force (F') needed to activate slip in the presence of cavities; (d) hinge point shift to next ligament.

References

1. Byun T.S., Hashimoto N., Farrell K., Lee E.H. *Characteristics of microscopic strain localization in irradiated 316 stainless steels and pure vanadium*. J. Nucl. Mater. **2006**, 349 (3), 251-264.
2. English C. and Hyde J. *Radiation Damage of Reactor Pressure Vessel Steel*. Comprehensive Nuclear Materials; Konings, R.; Stoller, R., Eds.; Elsevier: Oxford, UK, **2012**; Volume 3, pp. 169-196, Chapter 3.
3. Xu, S.X.; Griffiths, M.; Scarth, D.A.; Graham, D. *Microstructure-based Polycrystalline Finite Element Modeling of Inconel X-750 Irradiated in a CANDU Reactor*. Engineering Fracture Mechanics, 2022, 276A,108814.
4. Adamson, R.B.; Coleman, C.E.; Griffiths, M. *Irradiation creep and growth of zirconium alloys: A critical review*. J. Nucl. Mater. **2019**, 521, 167-244.
5. Griffiths, M. *Microstructural Effects on Irradiation Creep of Reactor Core Materials*. Materials **2023**, 16, 2287. https://doi.org/10.3390/ma16062287
6. Christodoulou, N., Levi, M.R., Turner, P.A. et al. Anisotropy of yielding in a Zr-2.5Nb pressure tube material. Metall. Mater. Trans. **2000**, A 31, 409–420.
7. Gussev M.N., Field K.G., Busby J.T., *Deformation localization and dislocation channel dynamics in neutron-irradiated austenitic stainless steels*, J. Nucl. Mater. **2015**, 460, 139-152.

8. Stephenson, K.J., Was G.S., The role of dislocation channeling in IASCC initiation of neutron irradiated stainless steel, J. Nucl. Mater. **2016**, 481, 214-225.
9. Byun, T.S., Hashimoto, N., Farrell, K. Deformation mode maps for tensile deformation of neutron-irradiated structural alloys, J. Nucl. Mater. **2006**, 351, 303-315.
10. Stroh A. N., *The formation of cracks as a result of plastic flow*. Proceedings of the Royal Society of London. Series A. Mathematical and Physical Sciences, **1954**, 223A, 404-414. https://doi.org/10.1098/rspa.1954.0124
11. Jiao, Z., Busby J.T., Was, G.S. *Deformation microstructure of proton-irradiated stainless steels*, J. Nucl. Mater. **2007**, 361, 218-227.
12. Howard C., Bhakhri V., Dixon C., Rajakumar H., Mayhew C., Judge C.D. *Coupling multi-scale mechanical testing techniques reveals the existence of a trans-granular channel fracture deformation mechanism in high dose Inconel X-750*, J. Nucl. Mater. **2019**, 517, 17-34.
13. Braski D.N. The effect of neutron irradiation on vanadium alloys, J. Nucl. Mater. 1986, 141-143, 1125-1131.
14. Griffiths, M.; Xu, S.; Ramos Nervi, J.E. Swelling and He-Embrittlement of Austenitic Stainless Steels and Ni-Alloys in Nuclear Reactors. Metals **2022**, 12, 1692. https://doi.org/10.3390/met12101692.
15. Changizian, P.; Yao, Z.; Long, F.; Topping, M.; Xu, S.X.; Daymond, M.R.; Griffiths, M. Mechanical behavior of recrystallized and precipitation-hardened Inconel X-750 before and after helium-implantation. Mater. Charact. 2023, 199, 112810.